



Cite this: DOI: 10.1039/coxx00000x

www.rsc.org/xxxxxx

ARTICLE TYPE

# ***In vivo* imaging of tumour bearing near infrared fluorescence- emitting carbon nanodots derived from tire soot**

Hae Young Ko<sup>a,††</sup>, Young Wook Chang<sup>a,††</sup>, Gokul Paramasivam<sup>a</sup>, Myoung Seok Jeong<sup>a</sup>, Sujeong Cho<sup>a</sup> and Soonhag Kim<sup>a\*</sup>

Received (in XXX, XXX) Xth XXXXXXXXX 20XX, Accepted Xth XXXXXXXXX 20XX

DOI: 10.1039/b000000x

**Carbon nanodots purified from the tire soot clearly visualized NIRF imaging of glioma *in vitro* and *in vivo*.**

Carbon-based nanomaterials, which include carbon nanotubes, fullerenes, and nanofibers, have promising applications in nanotechnology, biosensing, and drug delivery<sup>1</sup>. More recently, carbon nanoparticles such as carbon nanodots (C-dots), have received great attention in the field of *in vivo* fluorescence imaging of living animals due to their unique emission properties and have been attracted an incredible research interest owing to their lower toxicity, good bio-compatibility, excellent water solubility, versatile surface modification, optical stability and green synthetic route<sup>2</sup>. Until now, most of the reported C-dots emit the blue to green fluorescence, and they usually exhibit excitation wavelength-dependent fluorescence<sup>3</sup>. Since the near-infrared fluorescence (NIRF) spectrum has low absorption in *in vivo* image<sup>4</sup>, development of NIR-emitting C-dots is very critical for the application of molecular imaging. Regrettably, few C-dots have been reported for the red or NIR region emission with any raise expectations<sup>5</sup> and none of the study has reported *in vivo* cellular imaging using NIR-emitting C-dots. The fluorescent C-dots have been studied with good preparative methods and separation techniques. Several common methods in making fluorescent carbon nanoparticles include high-energy ion beam radiation<sup>6</sup>, laser ablation<sup>7</sup>, thermal decomposition<sup>8</sup>, electrooxidation<sup>9</sup> and oxidation with nitric acid<sup>8(b)</sup>. Among all these synthetic methods, the soot-based approach is simple and straight forward.

Herein, we reported a preparing and isolating fluorescent C-dots from tire soot (designated as tC-dots) by means of an oxidative acid treatment with nitric acid and demonstrated NIRF property of the tC-dots using C6 (a rat glioma cell line) cells *in vitro* and *in vivo*.

The tC-dots were prepared as depicted in Figure 1. Briefly, the tire soot was collected from the combustion of several tire pieces. 100 mg of the soot was mixed with 5 M nitric acid and refluxed at 120 °C for 12 h by direct thermal oxidation method. The separation of particles was followed by centrifugation and dialysis. The fluorescence spectra of the tC-dots showed strong absorbance at 280 nm and the highest fluorescence intensity was achieved at the excitation wavelength of 420 nm, which showed an emission maximum



**Figure 1.** Schematic diagram of synthesizing the tC-dots from tire soot.

at 520 nm (Figure S1†). The fluorescence intensity of the tC-dots in the pH range from 3 to 10 did not change significantly, implying that the tC-dots will be useful for imaging cells at the physiological and pathological pH range of 4.5–9.5 (Figure S2†)<sup>10</sup>. The emission spectra of the tC-dots were broad ranging from 430 to 710 nm with a dependence on the excitation wavelengths ranging from 340 to 660 nm, while the intensity of the emission peak was decreased with increasing excitation wavelengths (Figure 2a and Table S1†). In addition, the optical stability of the tC-dots was better than one of the traditional dye, FAM (Figure S3†). Transmission electron microscopy (TEM) images were acquired to identify the morphology and particle size distribution of the tC-dots. The diameter of the tC-dots was  $11 \pm 3$  nm with a broad size distribution ranged 8–15 nm, which is the general pattern of C-dots size distribution causing the broad range of emission spectra (Figure 2b and Figure S4†)<sup>7</sup>. The high-resolution TEM image from the inset of Figure 2b displayed crystalline patterns in the tC-dots. The X-ray photoelectron spectroscopy (XPS) for the elemental composition of the tC-dots demonstrated that the atomic percentage of C, O, N and Si were 31, 58, 2 and 9 %, respectively (Figure S5†). Unfortunately, relatively high composition of Si from the tC-dots was obtained due to a glass substrate used during the preparation of XPS sample. Three carbon atom peaks, C–C, C–O and C=O were clearly absorbed at 284.7, 286.4 and 288.8 eV, respectively (Figure S6†). It was noted that the energy peak at 284.7 eV acquired by a high-resolution XPS confirmed a predominant composition of sp<sup>2</sup> carbon in the tC-dots that is frequently found in general C-dots as a source of graphitic structure of the tC-dots<sup>11</sup>. In addition, the tC-dots analyzed by fourier transform infrared spectroscopy (FTIR) and Raman spectroscopy. FTIR possessed various surface functional groups including OH, C=O and COOH (Figure S7†). Raman analysis of the tC-dots clearly showed 2 different bands at 1590 and 1320 cm<sup>-1</sup> indicating G and D band which are known as the general property of the C-dots

(Figure S8†)<sup>9(b)</sup>.

To investigate the feasibility of imaging NIRF signals using the tC-dots in C6 cells, 200  $\mu$ l of the tC-dots (1 mg/ml) was taken in a microtube and a fluorescence imaging was performed by the IVIS spectrum imaging system. The spectral tube imaging of the tC-dots with various excitation wavelengths including 430, 465, 500, 535, 570, 605, 640, 675, and 710 nm was clearly visualized with their corresponding spectral emission wavelengths including 500, 520, 540, 560, 580, 600, 620, 640, 660, 680, 700, 720, 740, 760, 780, and 800 nm, respectively (Figure S9†). The NIR fluorescence intensity of the tC-dots was successfully acquired even at the excitation wavelength more than 640 nm. However, fluorescence intensity of the region of interest (ROI) from the spectral tube imaging showed gradually decreased NIRF emission signals ranging from 700 to 800 nm with increasing excitation wavelengths. To further confirm NIRF property of the tC-dots in cells, cellular viability of the tC-dots was first conducted in C6 cells. Various concentrations (0, 20, 40, 100, 200 and 400  $\mu$ g/ml) of the tC-dots showed no significant reduction in cellular viability of C6 cells (Figure S10†). Confocal microscopy analysis demonstrated that the tC-dots easily entered into C6 cells without any further functionalization on the surface of the tC-dots (Figure 3a). Furthermore, the brightness of spectral fluorescence imaging at various excitation wavelengths (488, 514, 543 and 633 nm) and emission filters (508-540, 561-604 and 636-700 nm) was clearly visualized in C6 cells incubated with the tC-dots (20  $\mu$ g/ml) for 3 h at 37  $^{\circ}$ C while C6 cells that did not undergo incubation with the tC-dots, to serve as a control, did not show any significant fluorescence activity (Figure S11†). Although the NIRF intensity was decreased as increasing excitation wavelengths, the NIRF brightness with 633 nm of excitation wavelength and 636-700 nm of emission filter was clearly detected comparing with fluorescence signals of the control. Interestingly, the fluorescence intensity of the tC-dots treated-C6 cells from the Figure 3a was still stable for 6 months (Figure S12†).

To conduct *in vivo* NIRF imaging of glioma, 200  $\mu$ l of the tC-dots (1mg/ml) was first incorporated with a matrigel. The matrigel with and without (used as background signals) the tC-dots was subcutaneously implanted into a left thigh and a right thigh of a nude mice, respectively. The fluorescence imaging of the mice with a pair of excitation and emission wavelengths including 535/600, 570/640, 605/660, 640/700, 675/740 and 710/800 nm displayed stronger fluorescence signal from the left thigh of the mice bearing the tC-dots-incorporated matrigel than the background signals from the right thigh containing the matrigel without the tC-dots (Figure S13†). However, *in vivo* imaging of the tC-dots from the left thigh with relatively short emission wavelengths at 520, 540 and 560 nm was visualized with difficulty due to high autofluorescence signals. Although the fluorescence emission intensity of *in vivo* imaging from the tC-dots-incorporated matrigel was weaker at longer excitation wavelengths, *in vivo* imaging of the tC-dots with NIR emission wavelengths including 660, 700, 740 and 800 nm showed a sensitive fluorescence activity from the left thigh with significant

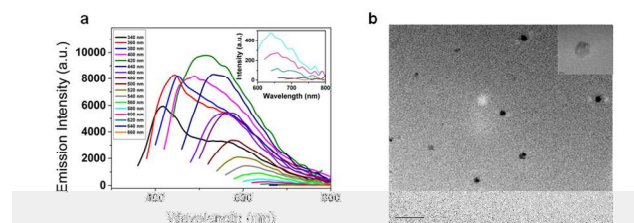


**Figure 2.** a) Emission spectra of the tC-dots. Emission spectra of the tC-dots were recorded for progressively longer excitation wavelengths from 340 to 660 nm in 20 nm increments. The inset is the magnification of emission spectra of excitation wavelength from 580 to 660 nm. b) TEM image of the tC-dots. The scale bar is 50 nm. The inset is the HR-TEM image of a single tC-dot (the scale bar is 5 nm for the inset).

decrease in tissue autofluorescence background (Figure S14†). Second, 200  $\mu$ g/ml of the tC-dots was incubated with  $1 \times 10^7$  of C6 cells for 3 h at 37  $^{\circ}$ C in a microtube. Although fluorescence emission activity with short excitation wavelengths at 430, 465, 500, 535 and 570 nm was clearly and strongly observed in the microtube of C6 cells both with and without (used as background signals) the incubation of the tC-dots, the NIRF brightness from the tube containing the C6 cells incubated with the tC-dots with excitation lights of 605, 640, 675 and 710 nm visualized clear signal separation from the background noise acquired from the cells only and buffers only in the tube (Figure S15†). The C6 cells with and without (used as background signals) the uptake of the tC-dots were then subcutaneously implanted into a right thigh and a left thigh of a nude mice, respectively. Similarly, the *in vivo* imaging of the subcutaneously injected C6 cells bearing the tC-dots was acquired with a broad range of excitation wavelengths from the right thigh of the mice and the fluorescence intensity was decreased at longer excitation wavelengths (Figure 3b). Although tissue autofluorescence background of *in vivo* imaging for C6 cells bearing the tC-dots was higher than that for *in vivo* imaging of the tC-dots, the relatively strong fluorescence signal separation from the tissue background and background signals from the right thigh were observed consistently with emission wavelengths of 660, 700, 740 and 800 nm (Figure S16†). The *ex vivo* tissue imaging from the mice bearing the tC-dots in the matrigel or C6 cells for the same excitation and emission with *in vivo* imaging of the tC-dots further confirmed the optical properties of the tC-dots including emission light with a broad range of excitation wavelengths, a decrease in emission intensity at longer excitation wavelengths and a high signal to background ratio with NIRF emission wavelengths (Figure S17†).

In this study, the successful synthesis of NIRF-emitting tC-dots was prepared by the oxidation with nitric acid. The physical characterization of the tC-dots, having broad size distribution ranging 8 to 15 nm and mainly composing of graphitic carbon core ( $sp^2$ ), displayed multi-colour fluorescent activity with NIRF property and a decrease in the fluorescence intensity of the emission peak with increasing excitation wavelengths from *in vitro*, *in vivo* and *ex vivo* imaging. As an aside, the tC-dots had highly self-promoted uptake into C6 cells without any further functionalization on the surface of the nanoparticles. The exact fluorescence mechanism from C-dots is still being explored. However, Eda *et al.* reported that the photo emissive band gaps of nano-sized  $sp^2$  carbon core

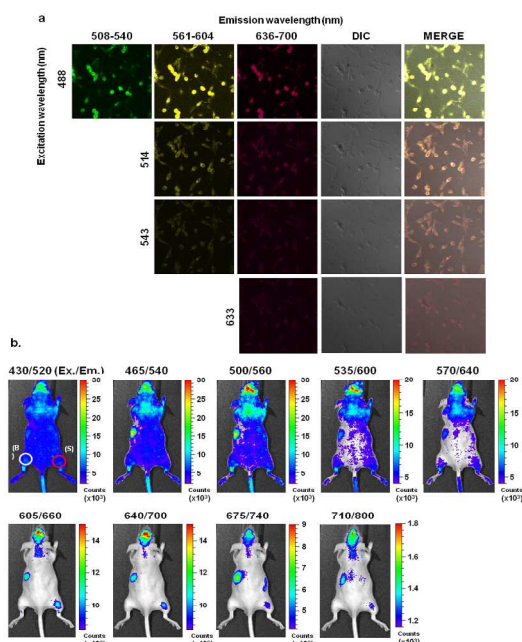


**Figure 3.** a) Confocal microscopy image of the tC-dots in C6 cells with excitation at 488 (1<sup>st</sup> row), 514 (2<sup>nd</sup> row), 543 (3<sup>rd</sup> row) and 633 nm (4<sup>th</sup> row) and emission filter of 508-580 (1<sup>st</sup> column), 561-593 (2<sup>nd</sup> column) and 636-700 nm (3<sup>rd</sup> column). DIC shows the bright field image for cellular morphology. b) *In vivo* fluorescence imaging of C6 cells bearing the tC-dots. The C6 cells with and without incubation of 200 µg/ml of the tC-dots was subcutaneously implanted into a right thigh (indicated by a red circle and an S) and a left thigh (indicated by a white circle and a B) of a nude mice, respectively (n=3).

cause fluorescence property of C-dots<sup>12</sup>. The broad range of emission spectra of the tC-dots with various excitation wavelengths resulted from the broad size distribution of the nanoparticles<sup>11</sup>. The observed reduction pattern of the emission light from the tC-dots with the increasing excitation wavelength could be correlated to the presence of very low elemental compositions of nitrogen and oxygen on the surface traps of the tC-dots<sup>13</sup>. Based on the physical fluorescence property of quantum confinement, the emission energy of fluorescent nanoparticles depends on the size of the nano core and the larger size of the nano core will be responsible for the NIR emissions<sup>3(c)</sup>. The diameter of most of C-dots emitting the blue to green fluorescence has been reported to be less than 10 nm<sup>2</sup>. Therefore, the diameter of the tC-dots ranging 8 to 15 nm could be one of the evidences for the NIRF property.

Although the optical properties of C-dots including size and morphology should be further studied relating to the efficiency of cellular uptake and distribution in cells, NIR property from the tC-dots will no doubt lead to more research in the field of *in vivo* molecular imaging and biomedical studies for the diagnosis and therapy of diseases. Since the quantum yield of C-Dots has been known to be very low<sup>14</sup>, surface passivation on the tC-Dots with PEG which provides strong photoluminescence will be helpful for NIRF imaging.

**Acknowledgment.** This work was supported by the Bio & Medical Technology Development Program of the National Research Foundation (NRF) funded by the Korean government (MEST) (No. 2011-0019270) and a grant of the Korea Healthcare technology R&D Project, Ministry of Health and Welfare (A120254)

## Notes and references

<sup>a</sup> Department of Biomedical Science, CHA University, 605-21 Yoeksam 1-dong, Gangnam-gu, Seoul, Korea. Tel.: +82-2-555-5063, fax: +82-2-3468-3373, \*E-mail address: kimsoonhag@empal.com

† Electronic Supplementary Information (ESI) available: Supplementary figure, table and experimental procedures are available in the ESI. See DOI: 10.1039/b000000x/

†† These authors contributed equally to this work

- (a) T. D. Burchell, in *Carbon materials for advanced technologies*, Pergamon Press, Amsterdam, 1999; (b) O. A. Shenderova, V. V. Zhirmov and D. W. Brenner, *Crit. Rev. in Solid State Mater. Sci.*, 2002, **27**, 227-236; (c) H. O. Pierson, in *Handbook of carbon, graphite, diamond and fullerenes: properties, processing and applications*, William Andrew Publishing/Noyes, Park Ridge, 1993.
- (a) S. N. Baker and G. A. Baker, *Angew. Chem.*, 2010, **49**, 6726-6744; (b) C. G. Joaquim, E. D. Silva and H. M. R. Gonçalves, *TrAC. Trends in Analytical Chemistry*, 2011, **30**, 1327-1336.
- (a) H. Zheng, Q. Wang, Y. Long, H. Zhang, X. Huang and R. Zhu, *Chem. Commun.*, 2011, **47**, 10650-10652; (b) S. Srivastava and N. S. Gajbhiye, *ChemPhysChem*, 2011, **12**, 2624-2632; (c) X. Wen, P. Yu, Y. Toh, Y. Lee, A. Hsu and J. Tang, *Appl. Phys. Lett.*, 2012, **101**, 163107-163111.
- P. D. Sima and J. R. Kanofsky, *Photochem. Photobiol.*, 2000, **71**, 413-421.
- (a) X. Guo, C. F. Wang, Z. Y. Yu, L. Chen and S. Chen, *Chem. Commun.*, 2012, **48**, 2692-2694; (b) F. Wang, M. Kreiter, B. He, S. Pang and C. Y. Liu, *Chem. Commun.*, 2010, **46**, 3309-3311.
- (a) A. D. A. Gruber, C. Tietz, L. Fleury, J. Wrachtrup and C. V. Borczyskowski, *Science*, 1997, **276**, 2012-2014; (b) F. Neugart, A. Zappe, F. Jelezko, C. Tietz, J. P. Boudou, A. Krueger and J. Wrachtrup, *Nano Lett.*, 2007, **7**, 3588-3591; (c) A. Batalov, V. Jacques, F. Kaiser, P. Siyushev, P. Neumann, L. J. Rogers, R. L. McMurtrie, N. B. Manson, F. Jelezko and J. Wrachtrup, *Phys. Rev. Lett.*, 2009, **102**, 195506.
- (a) Y. P. Sun, B. Zhou, Y. Lin, W. Wang, K. A. Fernando, P. Pathak, M. J. Mezziani, B. A. Harruff, X. Wang, H. Wang, P. G. Luo, H. Yang, M. E. Kose, B. Chen, L. M. Veca and S. Y. Xie, *J. Am. Chem. Soc.*, 2006, **128**, 7756-7757; (b) L. Cao, X. Wang, M. J. Mezziani, F. Lu, H. Wang, P. G. Luo, Y. Lin, B. A. Harruff, L. M. Veca, D. Murray, S. Y. Xie and Y. P. Sun, *J. Am. Chem. Soc.*, 2007, **129**, 11318-11319.
- (a) B. R. Selvi, D. Jagadeesan, B. S. Suma, G. Nagashankar, M. Arif, K. Balasubramanyam, M. Eswaramoorthy and T. K. Kundu, *Nano Lett.*, 2008, **8**, 3182-3188; (b) A. B. Bourlinos, A. Stassinopoulos, D. Anglos, R. Zboril, V. Georgakilas and E. P. Giannelis, *Chem. Mater.*, 2008, **20**, 4539-4541.
- (a) T. Schroeder, *Nature*, 2008, **453**, 345-351. (b) J. Lu, J. Yang, J. Wang, A. Lim, S. Wang and K. P. Loh, *ACS Nano*, 2009, **3**, 2367-2375.
- J. R. Casey, S. Grinstein and J. Orlowski, *Nat. Rev. Mol. Cell Biol.*, 2010, **11**, 50-61.
- S. C. Ray, A. Sha, N. R. Jana and R. Sarkar, *J. Phys. Chem.*, 2009, **113**, 18546-18551.
- G. Eda, Y. Y. Lin, C. Mattevi, H. Yamaguchi, H. A. Chen, I. S. Chen, C. W. Chen and M. Chhowalla, *Adv. Mater.*, 2010, **22**, 505-509.
- M. J. Krysmann, A. Kelarakis, P. Dallas and E. P. Giannelis, *J. Am. Chem. Soc.*, 2012, **134**, 747-750.
- H. P. Liu, T. Ye and C. D. Mao, *Angew. Chem. Int. Ed.*, 2007, **46**, 6473-6475.

